ACCSCIENCE PUBLISHING

Materials Science in Additive Manufacturing

ORIGINAL RESEARCH ARTICLE

Biomimetic-enhanced metamaterial with improved compression energy absorption in three orthogonal directions

Zhonggang Wang[1,2], Lejiang Wang[1,2], Ziping Lei[1,2], Ruochao Zhao[1,2], Kai Liu[1,2*], and Xinxin Wang[1,2,3*]

[1]School of Traffic & Transportation Engineering, Central South University, Changsha, Hunan, China

[2]The State Key Laboratory of Heavy-Duty and Express High-Power Electric Locomotive, Changsha, Hunan, China

[3]Department of Mechanical Engineering, National University of Singapore, Singapore

Abstract

Achieving a balanced enhancement of mechanical properties across different loading directions remains a fundamental challenge in the design of advanced cellular structures. In this study, a novel multi-biomimetic design strategy is proposed by integrating three biomimetic designs: honeycomb arrays, tortoise shell microarchitecture, and the skeletal framework of deep-sea glass sponges. This hybrid design approach reinforces both edges and nodes, enabling superior mechanical response under multi-directional compressive loading. Specimens were fabricated via selective laser melting using 6061 aluminum alloy, and the mechanical characterizations were performed through quasi-static compression experiments and finite element analysis. Relative to conventional honeycombs, biomimetic-enhanced structures demonstrated a 15.37% improvement in specific energy absorption (SEA) under out-of-plane compression, with a more pronounced enhancement of up to 65.23% under in-plane compression. This performance improvement is attributed to the increased vertically oriented members along the loading axis. The biomimetic-enhanced structures exhibit a multi-zone distributed deformation mode while sustaining progressive global collapse, yielding a more homogeneous stress distribution and prolonged energy dissipation plateau. The data-driven parametric analysis was conducted to quantify the mapping relationships between key geometric parameters and critical crashworthiness indicators. This enabled the identification of optimized structural configurations with maximized SEA. The proposed multi-biomimetic framework offers broad applicability in impact protection engineering.

Keywords: Mechanical metamaterial; Bio-inspired design; Compression performance; Energy absorption; Deformation mechanism

***Corresponding authors:**
Kai Liu
(liu_kai@csu.edu.cn);
Xinxin Wang
(csuwxx@csu.edu.cn)

Citation: Wang Z, Wang L, Lei Z, Zhao R, Liu K, Wang X. Biomimetic-enhanced metamaterial with improved compression energy absorption in three orthogonal directions. *Mater Sci Add Manuf.* 2026;5(3):026150027. doi: 10.36922/MSAM026150027

Received: April 7, 2026

Revised: May 14, 2026

Accepted: May 22, 2026

Published online: June 19, 2026

1. Introduction

Over the course of long-term evolution, nature has developed a rich diversity of biological structures with exceptional functional characteristics, including low density, high strength-to-weight ratio, efficient energy dissipation, and adaptive multifunctionality.[1-4]

These natural architectures achieve outstanding mechanical performance through intricate, multi-scale, and highly ordered geometric morphologies.[5-9] Critically, they embody a design paradigm of trading structural configuration for enhanced functionality, offering profound inspiration for advanced engineering materials and structural systems.

In modern engineering practice, structural materials are increasingly required to be lightweight, high in specific strength and stiffness, and capable of efficient energy absorption. This is particularly evident in transportation, aerospace, civil defense, and marine engineering—domains where components must perform reliably under complex loading conditions, including impact, vibration, thermal gradients, and coupled environmental loads.[10-12] Conventional monolithic materials, despite their high intrinsic strength, are often limited by excessive mass, poor energy absorption, and low functional tunability. They therefore struggle to simultaneously satisfy competing demands such as lightweight design, crashworthiness, and multifunctional integration. In response, biomimetic honeycomb materials, created by abstracting and adapting nature's optimized structural motifs, have emerged as a prominent research frontier in advanced structural materials.[13-15]

Recent studies have demonstrated that the mechanical performance of honeycomb-based metamaterials can be substantially improved through hierarchical design, auxetic transformation, bio-inspired geometric modulation, and advanced manufacturing routes.[16] Some aperiodic lattice metamaterials also exhibit remarkable mechanical improvements.[17-19] Current research is evolving from conventional hexagonal honeycombs toward multiscale, reinforced, chiral, and multifunctional cellular architectures, with emphasis on lightweight design, crashworthiness, and tunable deformation mechanisms.[20-24] Hierarchical honeycombs have been widely investigated, as the introduction of subcells can redistribute stress, trigger progressive collapse, and improve specific energy absorption. Auxetic and chiral systems (such as hierarchical anti-tetrachiral structures and additively manufactured negative-Poisson's-ratio architectures) have attracted increasing attention due to their rotation-dominated deformation, reduced peak stress, and enhanced impact resistance.[24-26] Origami- and kirigami-inspired honeycombs have further been proposed to tailor collapse paths and improve multidirectional energy absorption, while biomimetic multi-cell composite tubes demonstrated the potential of combining biological prototypes with hierarchical load-transfer mechanisms.[27-30] Nevertheless, most existing studies rely on single-source biomimetic inspiration or single-scale reinforcement strategies. Triply periodic minimal surface (TPMS) lattice were fabricated using laser powder bed fusion (LPBF) technology, demonstrating the significant application potential of nickel-titanium alloys based on three-period minimal surface lattice metamaterials.[31] Cellular structures fabricated via additive manufacturing have been discussed, providing insights and prospects for the future development of fatigue-resistant additively manufactured cellular materials.[32] The synergistic enhancement of both cell walls and nodal regions, combined with experimentally validated compressive behavior across three orthogonal directions, remains insufficiently explored.

Different from the studies discussed above, this work proposes a multi-biomimetic design strategy that draws inspiration from three distinct biological designs (including honeycomb arrays, tortoise shell microarchitecture, and deep-sea glass sponge skeletal frameworks) to achieve synergistic reinforcement of both cell edges and nodal regions. The biomimetic honeycomb metamaterials were fabricated using selective laser melting (SLM) additive manufacturing technology with 6061 aluminum alloy (Al 6061). The compressive behavior along three orthogonal directions were characterized through quasi-static experiments and finite element simulations, and a data-driven framework was introduced to establish quantitative structure–property relationships. This study contributes a replicable biomimetic design paradigm for lightweight energy-absorbing structures and advances the understanding of additively manufactured metamaterials under multi-directional loading.

2. Materials and methods

2.1. Design principle

The original concept is developed through a tri-biomimetic coupling strategy, aiming to enhance both the edge and node regions of the unit simultaneously. As shown in Figure 1A, the design process begins with natural honeycomb and tortoise shell. The natural honeycomb provides a basic hexagonal topology, which has advantages such as high material efficiency and stable load transfer capability.[33] The tortoise shell, with a large hexagon as its skeleton, is formed by extending lines from its vertices to mimic the shape of a tortoise shell.[34] The biomimetic honeycomb and tortoise shell structures are integrated, with the tortoise shell structure attached to the honeycomb unit wall, enhancing its edges (Figure 1B). This structure can improve the rigidity and load-bearing capacity of the edge-dominated framework while maintaining the lightweight and porous characteristics of the honeycomb.

Under external compressive loads, stress concentration and deformation localization often occur at the joints, making single edge reinforcement insufficient. Therefore, the third biomimicry was introduced (Figure 1C). The glass sponge system exhibits robust node connections and efficient stress distribution performance.[35] Considering the overlapping effect of staggered nodes, the node positions in the coupled framework were modified and replaced based on the skeleton characteristics of the deep-sea glass sponge system.[36] By integrating the third biomimicry structure into the already edge-enhanced topological structure, the final edge-node dual-enhanced structure was obtained (Figure 1D). The structure combines the geometric efficiency of honeycomb, the edge reinforcement effect of tortoise shell, and the mechanical performance advantages derived from the node reinforcement mechanism of the glass sponge skeleton system.

For comparison, Figure 1E and 1F show the conventional hexagonal honeycomb and the biomimetic-enhanced metamaterial specimens. Unlike conventional structures, the design features a multi-layered interwoven load transfer network, which can synergistically enhance the strength of both the edges and nodes of the unit. Therefore, this tri-biomimetic design provides strategies and guidance for developing lightweight cellular materials with higher stiffness, strength, and energy absorption performance.

2.2. Quasi-static compressions

The mechanical properties of the biomimetic-enhanced

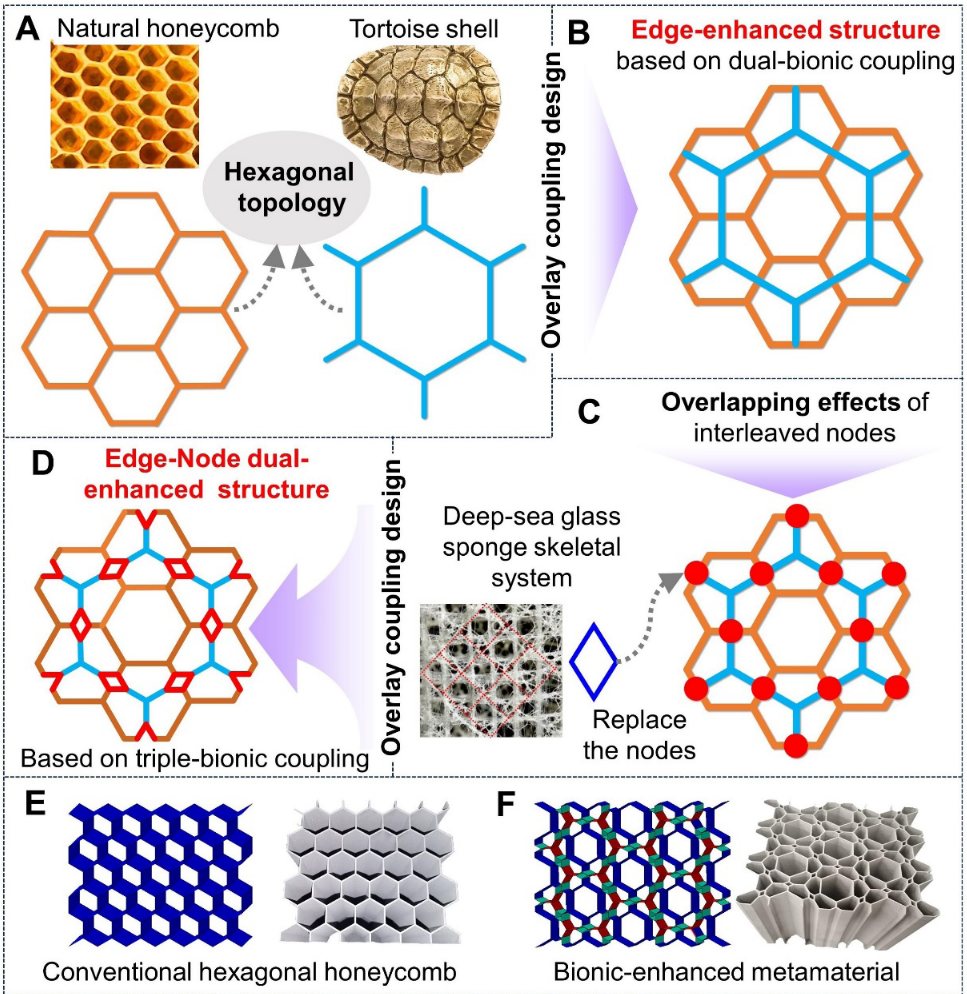

Figure 1. Design principle. (A) Conventional hexagonal topology; (B) Edge-enhanced structure based on dual-biomimetic coupling; (C) Introduction of biomimetic diamond-shaped structure; (D) Edge-Node dual-enhanced topology; (E) Conventional hexagonal specimens; (F) Present biomimetic-enhanced metamaterial specimens.

metamaterial were experimentally characterized via quasi-static uniaxial compression testing. Specimens were fabricated via selective laser melting (SLM) using 6061 aluminum alloy powder (particle size: 15–53 μm).[37] Prior to testing, the material parameters of 6061 aluminum alloy were calibrated for subsequent finite element simulations. Geometric specifications and fabrication parameters were controlled to ensure rigorous comparative analysis. The biomimetic-enhanced metamaterial specimens measured 91.635 mm × 105.720 mm × 100 mm with a wall thickness of 0.5 mm, while the conventional hexagonal honeycomb specimens measured 91.135 mm × 106.019 mm × 100 mm with a wall thickness of 0.782 mm. Both specimen types were manufactured to an identical mass of 256 g, ensuring fair comparison across structures. Compression testing was performed along three orthogonal directions to characterize the directional-dependent mechanical response.

The quasi-static compression experiments were carried out using an MTS Landmark universal testing machine. The test specimen is placed on the support platform template and loaded at a controlled strain rate of 0.001 s^{-1}. The maximum load capacity of the testing machine is 300 kN, with a measurement accuracy of ±0.5%. The deformation process was captured and recorded using a high-definition camera.

To accurately evaluate the optimization of energy absorption performance of the biomimetic-enhanced metamaterial compared to the conventional honeycomb, the specific energy absorption (SEA) was adopted as a representative indicator to describe the energy absorption capacity of materials. It is defined as follows:

$$\mathrm{SEA}=\frac{\int_{l_0}^{l_1}P(x)\,\mathrm{d}x}{m} \tag{1}$$

where $P(x)$ represents the compressive force at a given strain state before the densification stage, l_0 denotes the initial compression height (the initial compression height is zero), and l_1 corresponds to the height at the onset of densification. A higher SEA value indicates superior energy absorption capability of the material.[38-40]

In addition to exceptional energy absorption capacity, excellent load-bearing stability is also an essential characteristic of high-performance energy absorbers. To further describe the energy absorption performance of the biomimetic-enhanced metamaterial, the crash force efficiency (CFE) index was introduced to evaluate load-bearing stability, expressed as:

$$\mathrm{CFE}=\frac{\mathrm{MCF}}{\mathrm{PCF}} \tag{2}$$

where PCF refers to the peak crushing force during the loading process, and MCF represents the mean crushing force, calculated as:

$$\mathrm{MCF}=\frac{\int_{l_0}^{l_1}P(x)\,\mathrm{d}x}{l_0-l_1} \tag{3}$$

The CFE reflects the stability of the structure during energy absorption and the uniformity of the load-displacement curve. A CFE value approaching 1 is indicative of a more stable load-bearing process. The SEA and CFE of the biomimetic-enhanced metamaterial under out-of-plane and in-plane compression in three directions are illustrated in the accompanying figures. Compared with the conventional honeycomb, the biomimetic-enhanced metamaterial demonstrates significant improvement in energy absorption performance: SEA increased by 15.37% under out-of-plane compression, while the increases under in-plane compression in the two directions were as high as 30.38% and 65.23%, respectively.

Regarding the evaluation based on the CFE index, biomimetic-enhanced metamaterial also exhibits outstanding performance. As shown in the Figure 2, compared to the conventional honeycomb, its CFE values under triaxial loading are closer to 1. The most notable improvement is observed in the in-plane II direction, with an optimization of 139.56%, indicating that biomimetic-enhanced metamaterial possesses more stable and superior load-bearing capacity under external loading.

2.3. Finite element analysis

Geometric models of both the biomimetic-enhanced metamaterial and conventional hexagonal honeycomb were created using SolidWorks (Dassault Systèmes) with approximate dimensions of 90 mm × 105 mm × 100 mm. The models were subsequently meshed in Altair HyperMesh, followed by mesh convergence analysis in Abaqus with an element size of 1 mm. Material parameters used in the finite element simulations are listed in Table 1. In the simulation parameter settings, contact between the plates and specimens was defined with a friction coefficient of 0.15. The lower rigid plate is fully constrained, while the upper rigid plate is free in the compression direction but has no velocity or rotation in other directions, to ensure that the test behavior is fully simulated under real-world conditions. Compression simulations were conducted using Abaqus/Explicit. The wall thickness parameters were established under equivalent mass conditions as follows: 0.5

mm for biomimetic-enhanced metamaterial and 0.782 mm for hexagonal honeycomb (established under equivalent mass conditions). The specimens were positioned between two rigid plates, with the lower plate fully constrained and the upper plate moving along the vertical axis at 500 mm/s to apply compressive loading. Compression was terminated at 90% of the original specimen height. Dynamic explicit algorithm was employed to accurately capture the quasi-static compression behavior. The geometric design model has a discrepancy of no more than 2.5% compared to the test samples, which is within a reasonable range.

Table 1. Material parameters in FEA model

Parameters	Density	Young's modulus	Poisson's ratio	Yield stress
Value	2,700 kg/m^3	20 GPa	0.33	220 MPa

Abbreviation: FEA: Finite element analysis.

3. Results and discussion

3.1. Compressive behaviors

Figure 2 presents comparative engineering stress-strain curves for the biomimetic-enhanced metamaterial and conventional hexagonal honeycomb under quasi-static compression along three orthogonal directions. The three loading directions are denoted as: in-plane I (X direction), in-plane II (Y direction), and out-of-plane (Z direction). Table 2 shows the mechanical performance data of conventional honeycomb and biomimetic-enhanced metamaterial. The uniform strain of 0.48 is taken as the threshold for the compacted region; the plateau phase begins at the strain corresponding to the peak stress and ends at 0.48.

In-plane I direction (Figure 2A): During the initial linear elastic stage, the biomimetic-enhanced metamaterial exhibited a rapid increase in stress compared to hexagonal honeycomb. In the plateau stage, the stress curve of biomimetic-enhanced metamaterial was consistently higher than hexagonal honeycomb with characteristic stress fluctuations, indicating a load-bearing mechanism transition from hexagonal bending dominance to quadrilateral stretching dominance. The enhanced compressive response of the reinforced honeycomb structure is mainly attributed to the modified load-transfer paths, increased edge–node constraints and the formation of additional plastic hinge regions. These features promote a more progressive collapse process and improve the utilization of the cell-wall material. Geometric topologies of multi-component couplings provide the biomimetic-enhanced metamaterial structure with exceptional energy absorption capacity. For comparison, all structures were designed with the same relative density, indicating that the performance enhancement resulted from topological reinforcement rather than increased material usage. Quantitatively, the biomimetic-enhanced metamaterial demonstrated a 30.38% improvement in SEA and nearly 60% advantage in CFE compared to hexagonal honeycomb (Figure 2D and 2E), indicating superior load-bearing stability in the in-plane I direction.

In-plane II direction (Figure 2B): The elastic stages of both structures were nearly superimposed with negligible differences. As the structure gradually yields, the peak stress of biomimetic-enhanced metamaterial is 1.4 MPa, which is twice that of hexagonal honeycomb. Throughout the plastic collapse plateau stage, the stress curve of biomimetic-enhanced metamaterial remained significantly higher than hexagonal honeycomb. In contrast, the conventional honeycomb exhibited notably poorer energy absorption performance with more pronounced stress fluctuations. The SEA of biomimetic-enhanced metamaterial exceeded hexagonal honeycomb by 65.23%, while the CFE advantage reached nearly 1.5 times (Figure 2D and 2E), directly demonstrating the superior overall stability of biomimetic-enhanced metamaterial in resisting external loads in this direction.

Out-of-plane direction (Figure 2C): The elastic stages of both structures were nearly identical. However, the biomimetic-enhanced metamaterial reached yield stress earlier than hexagonal honeycomb and exhibited higher peak stress throughout. Notably, the stress curve of hexagonal honeycomb began to fluctuate at strain ~0.15 and gradually stabilized around strain 0.3, reflecting structural instability. In contrast, the curve of biomimetic-enhanced metamaterial remained noticeably smoother and more stable throughout the compression process. The SEA improvement ratio of biomimetic-enhanced metamaterial compared to hexagonal honeycomb was 15.37%, while the CFE advantage reached 16.76% (Figure 2D and 2E), indicating that biomimetic-enhanced metamaterial not only possesses superior energy absorption capacity but also exhibits greater stability when resisting external loads in the out-of-plane direction. Table 2 provides a comparison of key compression performance metrics obtained from finite element analysis (FEA) simulations with their experimental counterparts. The quantitative analysis reveals discrepancies of less than 8%.

3.2. Deformation modes

Deformation mode reflects the buckling evolution pattern of cellular structures under external compressive loading, which can reveal their stress distribution characteristics, energy dissipation mechanisms, and overall stability

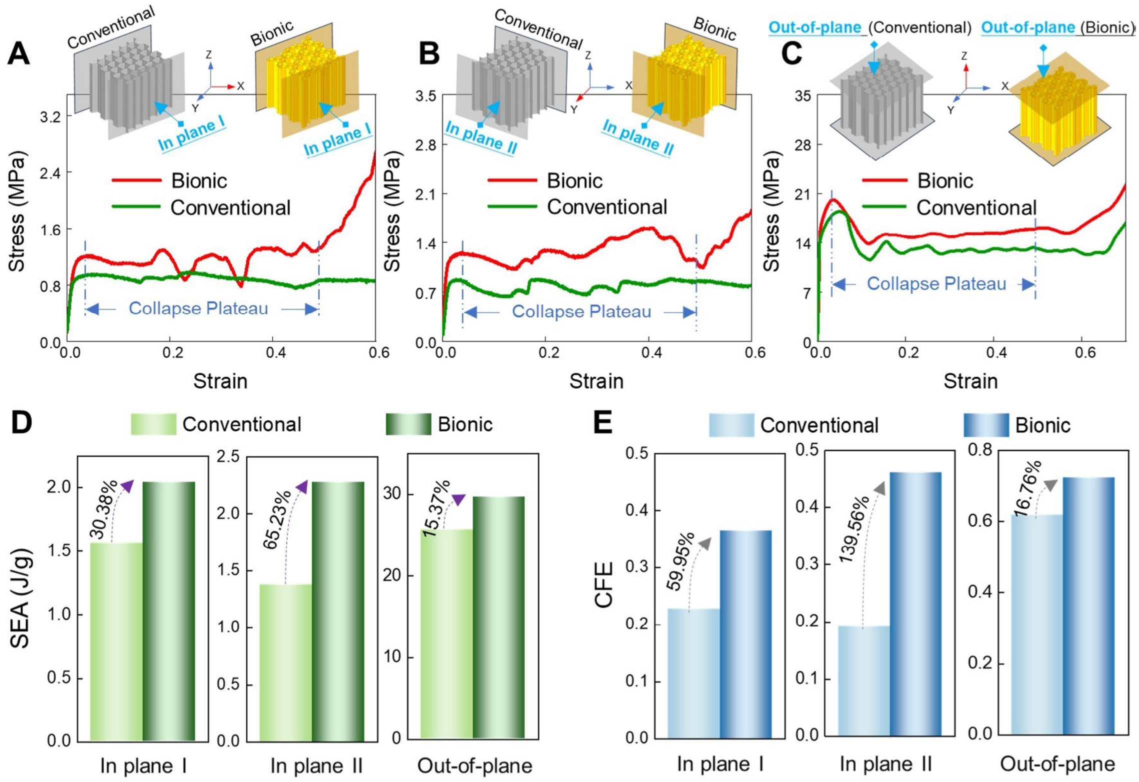

Figure 2. Mechanical properties. (A–C) Stress–strain curve in the in-plane I direction (A), the in-plane II direction (B), and the out-of-plane direction (C). (D) SEA comparison. (E) CFE comparison.
Abbreviations: CFE: Crash force efficiency; SEA: Specific energy absorption.

Table 2. Mechanical performance data of conventional honeycomb and biomimetic-enhanced metamaterial (experiment and simulation)

Type		Conventional honeycomb			Biomimetic-enhanced metamaterial		
Loading direction		In plane I	In plane II	Out-of-plane	In plane I	In plane II	Out-of-plane
SEA (J/g)	Exp.	1.57	1.38	25.74	2.04	2.27	29.7
	FEA	1.71	1.45	24.63	1.88	2.15	28.8
	Error	5.92%	3.43%	3.05%	5.66%	3.76%	2.13%
CFE	Exp.	0.23	0.19	0.62	0.36	0.46	0.72
	FEA	0.21	0.18	0.61	0.33	0.41	0.69
	Error	6.30%	3.75%	1.13%	6.03%	7.97%	2.95%
MCF (MPa)	Exp.	0.88	0.77	19.23	1.15	1.28	20.73
	FEA	0.96	0.82	20.88	1.05	1.21	21.05
	Error	6.03%	4.36%	5.70%	6.30%	3.90%	1.06%

Abbreviations: CFE: Crash force efficiency; FEA: Finite element analysis; MCF: Mean crushing force; SEA: Specific energy absorption.

performance. Figure 3 displays the deformation modes of hexagonal honeycomb and biomimetic-enhanced metamaterial at successive strain levels (0.15, 0.30, 0.45, and 0.60), together with corresponding simulation results. The cellular metamaterial dissipates energy primarily through bending and progressive collapse of cell walls under in-plane compression, while under out-of-plane compression, the main energy absorption mechanism is plastic deformation induced by buckling instability of the thin walls.

In-plane I direction: For hexagonal honeycomb (Figure 3A), external loading causes inclined cell walls to rotate, driving vertical walls to tilt and creating uneven stress distribution. As strain increases, localized collapse occurs at the bottom, with most cell walls eventually assuming horizontal or inclined orientations, severely compromising vertical load resistance. Conversely, the biomimetic-enhanced metamaterial (Figure 3B) exhibits a distinctive X-shaped load-bearing pattern (highlighted by red dashed circles). The center area of the X-pattern maintains a rectangular configuration without significant vertical wall rotation. The integrated large hexagonal framework weakens transverse influences on the small hexagonal cells, while the diamond-shaped edge structures stabilize the small hexagons by interrupting cell wall continuity. In Figure 3B, the finite element deformation of the in-plane I condition at 0.3 strain is enlarged for display. It can be observed that most of the stress is concentrated on the X-shaped strips, with the vertical members and diamond structures bearing most of the load. Multiple plastic hinges have formed in the diamond structures, playing a key role in distributing the external load. As strain progresses, triangular structures emerge within the deformed geometry. These triangular configurations provide superior structural stability, explaining the biomimetic-enhanced metamaterial's enhanced load-bearing performance compared to hexagonal honeycomb.

In-plane II direction: the hexagonal honeycomb undergoes arc-shaped deformation at both upper and lower ends (symmetric about the center), which gradually converge toward the core at higher strains, eventually reaching complete crushing. Although arc structures effectively disperse external loads, the high proportion of horizontal cell walls limits axial load resistance. Critically, central cells undergo minimal shape changes, indicating poor participation in Y-direction resistance—a localized, inefficient load-transfer mode. In contrast, the biomimetic-enhanced metamaterial exhibits coordinated three-layer deformation from initial loading (strain 0.15 onwards, evident at strain 0.30). The integrated large hexagonal geometry redirects stress from small hexagonal cell walls toward node positions, promoting

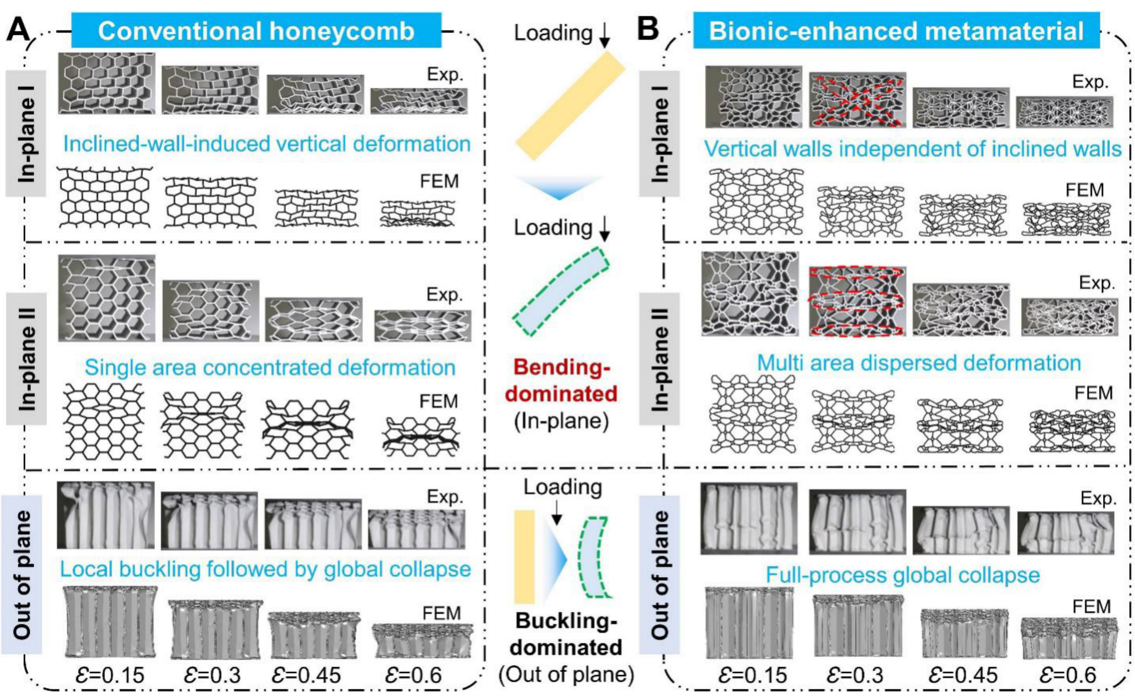

Figure 3. Compression deformation process. (A) Conventional honeycomb. (B) Biomimetic-enhanced metamaterial.

uniform deformation and a three-layer integrated load-resistance mechanism. The introduced diamond structures effectively disperse localized stress, reducing concentrated loads on large hexagonal walls while maintaining high proportions of vertical load-bearing elements. During deformation, the diamond structure fragments the small hexagonal regions into multiple triangular configurations, which form the primary load-bearing framework after the three-layer deformation stage. This integrated, multi-layer architecture renders the biomimetic-enhanced metamaterial substantially more stable and efficient in Y-direction resistance than hexagonal honeycomb.

Out-of-plane direction: the hexagonal honeycomb exhibits immediate localized buckling upon loading initiation (Figure 3A). At strain 0.15, distinct bending deformations appear at the upper-left and right vertical walls, indicating structural instability. By strain 0.30, progressive layered folding and wrinkling emerge from the compression zone, with energy primarily absorbed through these localized wrinkle formations. At higher strains, lower vertical walls undergo progressive bending and folding deformations until wall collapse terminates the plateau stage. In contrast, the biomimetic-enhanced metamaterial undergoes more distributed deformation (Figure 3B). Minor bending appears at multiple locations at strain 0.15, progressing to shear buckling at the central position by strain 0.30. This shear buckling deepens progressively with simultaneous inclination of edge vertical walls, resulting in holistic, uniform energy absorption. hexagonal honeycomb's localized bending concentrations create stress hotspots susceptible to concentration effects, whereas the biomimetic-enhanced metamaterial's distributed shear-buckling mechanism enables more uniform stress distribution. Combined with the superior specific energy absorption values (Figure 2E), the biomimetic-enhanced metamaterial demonstrates both higher capacity and more stable, global deformation behavior under Z-direction loading.

3.3. Parameter optimization

Figure 4 illustrates parameter optimization of the biomimetic-enhanced metamaterial through machine learning, evaluating two design variables: wall thickness (0.3–1.1 mm, 10 sampled values) and diamond proportion (0.25–0.50, 10 sampled values). Compression simulations were performed for 100 iterations in each of the three orthogonal directions. Gaussian Process Regression model was employed to process simulation data, with prediction accuracy assessed via scatter plots (Figure 4A). Predicted values align closely with experimental results along the diagonal, with most data points falling within the error bands. Statistical metrics confirm strong model fidelity: first objective ($R^2 \approx 0.943$, Spearman ≈ 0.945); second objective ($R^2 \approx 0.938$, Spearman ≈ 0.935); third objective ($R^2 \approx 0.951$, Spearman ≈ 0.944). All R^2 values exceed 0.94, indicating robust explanatory power for target response variance, while Spearman coefficients above 0.93 demonstrate accurate preservation of sample rank relationships. Low root mean square error (RMSE) and mean absolute error (MAE) values across all objectives indicate effective model generalization across disparate response scales. Marginal distribution plots confirm that predicted distributions consistently match actual distributions, demonstrating both local fidelity and global reconstruction capability within the sample space.

To quantify parametric contributions to model predictions, Shapley Additive Interpretation (SHAP) analysis was applied (Figure 4B). SHAP values indicate the marginal contribution of each parameter, with magnitude reflecting influence strength and sign indicating facilitative or inhibitory effects. Global importance analysis reveals that thickness dominates the first two objectives (81.9% and 84.9% respectively), substantially exceeding proportion's contribution. For the third objective, thickness contribution further increases to 94.5%, while proportion contributes only 5.5%. Under the current parameter space and objective definitions, thickness emerges as the primary controlling factor, while proportion functions as a secondary modulating parameter. The bee swarm plots display distributions of SHAP values across features, with color gradients distinguishing high and low feature values. Thickness exhibits a wider SHAP value distribution, indicating stronger positive or negative impacts on predictions, whereas proportion values concentrate within narrower ranges, signifying weaker, localized fine-tuning effects. Notably, thickness distributions vary across objectives, suggesting that while its dominance is consistent, the magnitude and functional form (potentially nonlinear) of its influence depend on the specific objective.

Response surface analysis (Figure 4C) reveals smooth gradient characteristics across the two-dimensional parameter space (thickness × proportion), with no severe oscillations or discontinuities in any of the three objectives. This indicates continuous objective-function mapping within the investigated parameter range and validates the appropriateness of Gaussian Process Regression modeling for characterizing smooth nonlinear responses. The principal gradient direction is controlled primarily by thickness, with proportion exerting secondary modulation effects. Based on Bayesian optimization with equal weighting across three directions, the globally optimal configuration was identified as follows: wall thickness

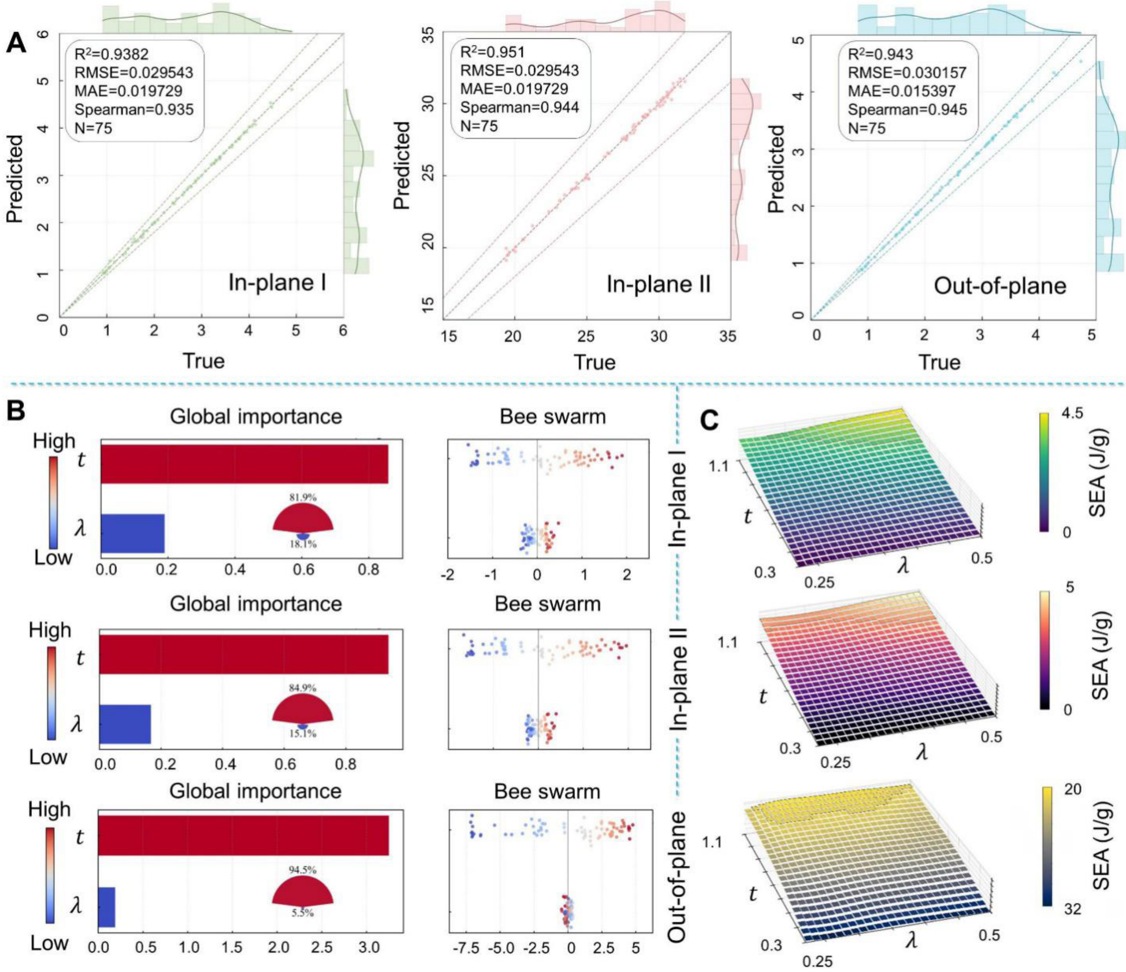

Figure 4. Machine learning parameter optimization. (A) Scatter plot. (B) Global importance bar chart. (C) Bee swarm plot.
Abbreviations: MAE: Mean absolute error; RMSE: Root mean square error.

of 0.95 mm and diamond proportion of 0.44. The corresponding three-directional SEA values are presented in Table 2.

3.4. Performance comparisons

Ashby plots enable systematic assessment of the performance-density relationship across diverse designs. They facilitate identification of performance-optimal structures and provide comprehensive benchmarking of mechanical properties relative to material density, thereby clarifying the competitive advantages and disadvantages of candidate structures. Figure 5 presents Ashby plots comparing the SEA of the biomimetic-enhanced metamaterial with existing structures under in-plane and out-of-plane compression conditions.

In-plane comparison (Figure 5A): The biomimetic-enhanced metamaterial achieves SEA exceeding 2 J/g at an equivalent density of 0.3 g/cm³. Relative to comparative structures, the self-locked chiral honeycomb (aluminum alloy, 0.05–0.2 g/cm³ density) demonstrates substantially lower performance with SEA of only 0.75–1 J/g, approximately one order of magnitude below the biomimetic-enhanced metamaterial.[41] The star-shaped honeycomb I has an equivalent density of 0.4 g/cm³, and its specific energy absorption hovers around 2 J/g. [42] Polymer-based structures demonstrate notably poorer energy absorption: hybrid honeycomb achieves 0.5–1 J/g at 0.1 g/cm³ density, re-entrant honeycomb ranges from 0.5–1.25 J/g at 0.25 g/cm³ density, and star-shaped honeycomb II spans the widest density range (0.3–0.5 g/cm³) with predominantly 1 J/g-level SEA.[43-46] The origami-lattice performs relatively well with SEA exceeding 1.5 J/g at 0.2 g/cm³ density. The corrugated honeycomb (steel, 0.1 g/cm³) exhibits superior SEA at equivalent density;

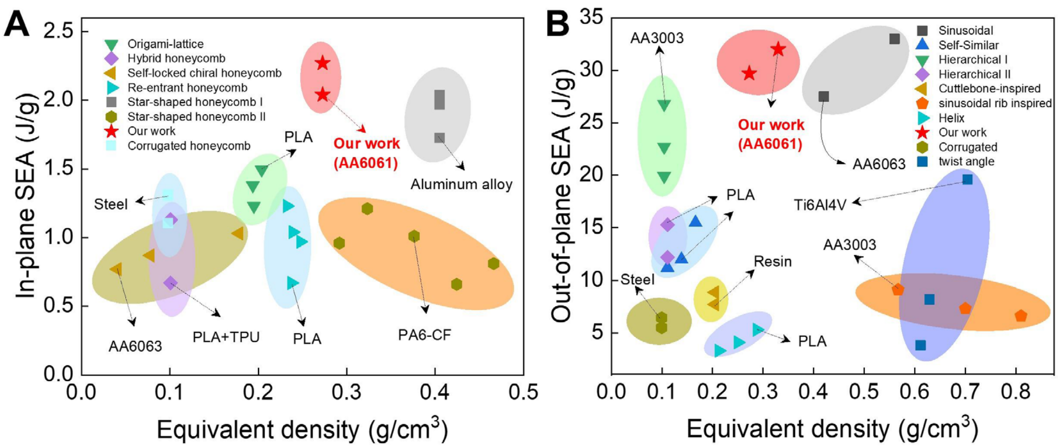

Figure 5. SEA comparison. (A) In-plane compression. (B) Out-of-plane compression.
Abbreviation: SEA: Specific energy absorption.

however, it remains inferior to the biomimetic-enhanced metamaterial's performance.[47]

Out-of-plane comparison (Figure 5B): The biomimetic-enhanced metamaterial significantly outperforms comparative structures with SEA exceeding 30 J/g at 0.3 g/cm³ density. Among aluminum alloy structures, hierarchical honeycomb I (AA3003, 0.1 g/cm³) achieves maximum SEA of approximately 26 J/g, while sinusoidal rib-inspired honeycomb (AA3003, 0.5–0.8 g/cm³) demonstrates substantially lower SEA of less than 10 J/g despite higher density.[48,49] High-strength materials show comparable or inferior performance: corrugated honeycomb (steel, 0.1 g/cm³) exhibits only 6 J/g SEA, and twist angle honeycomb (Ti6Al4V, 0.6–0.7 g/cm³) achieves maximum SEA of approximately 20 J/g.[47,50] Polymer materials (PLA and resin) demonstrate substantially lower SEA concentrated in the lower-left region of the diagram, indicating significant performance gaps.[51-53] The sinusoidal honeycomb fabricated from AA6063 material exhibits marginally higher SEA than the biomimetic-enhanced metamaterial; however, its equivalent density is approximately double that of the biomimetic-enhanced metamaterial, indicating superior mass-normalized energy absorption performance for the proposed structure.

4. Conclusion

In summary, this study proposes a design strategy for a novel metamaterial that enhances the weak areas of edges and nodes through three-level biomimetic approach. The mechanical behavior of the metamaterial under three-dimensional uniaxial compression load was explored through compressive experiments and simulations. Compared with conventional honeycomb of the same quality, the biomimetic-enhanced metamaterial has significantly improved its three-dimensional energy absorption capacity and deformation stability. By comparing SEA indicators, the biomimetic-enhanced metamaterial improved by 30.38%, 65.32%, and 15.37% in the in-plane I, in-plane II, and out-of-plane compression directions, respectively. By comparing the CFE indicators, the biomimetic-enhanced metamaterial improved by 59.95%, 139.56%, and 16.76% in the in-plane I, in-plane II, and out-of-plane compression directions, respectively. In addition, machine learning methods were used to perform multi-objective optimization on the biomimetic-enhanced structure under consistent three-dimensional compression weight. Based on Bayesian method and using SEA as the evaluation criterion, the optimal structural configuration was calculated, and it was found that the SEA value of biomimetic-enhanced metamaterial was the highest under the parameter structure with a thickness of 0.95 mm and a ratio of 0.44. The new structure proposed in this study has broad application prospects in engineering, and the coupled multi-biomimetic design strategy provides guidance for the future development of metamaterials.

Acknowledgments

The authors gratefully acknowledge the support provided by the Institute for Advanced Study and the High Performance Computing Center of Central South University.i ni

Funding

This work was financially supported the Science and Technology Program of Hunan Province (2025JK2067).

Conflict of interest

Xinxin Wang serves as Deputy Associate Editor of this journal, but was not in any way involved in the editorial and peer-review process conducted for this paper, directly or indirectly. The authors declare they have no competing interests.

Author contributions

Conceptualization: Zhonggang Wang, Xinxin Wang
Data curation: Lejiang Wang, Kai Liu
Formal analysis: Xinxin Wang, Ruochao Zhao
Investigation: Lejiang Wang, Ruochao Zhao
Methodology: Lejiang Wang, Ziping Lei
Writing–original draft: Zhonggang Wang, Lejiang Wang
Writing–review & editing: Xinxin Wang, Kai Liu

Ethics approval and consent to participate

Not applicable.

Consent for publication

Not applicable.

Availability of data

The data that support the findings of this study are available from the corresponding authors upon reasonable request.

References

1. Deng X, Lu Q, Cai Z, Zhang X. In-Plane Mechanical Properties of a Tetra-Missing Rib Symmetry Honeycomb. *Materials*. 2026;19(3):553.

   doi: 10.3390/ma19030553

2. Guo X, Wu M, Bu W, Lv P, Liang X. Star-Chiral Honeycomb with robust impact resistance. *Thin-Walled Struct*. 2026;222:114550.

   doi: 10.1016/j.tws.2026.114550

3. Li F, Huang W, Zhang Q, Wang Z. Concave–rhombic hybrid honeycomb structures: Energy absorption mechanism and multi-objective optimization. *Structures*. 2026;85:111202.

   doi: 10.1016/j.istruc.2026.111202

4. Guan P, Hao N, Wang P. Compressive behavior of 3D printed biomechanically inspired helicoidal honeycomb structures. *Int J Mech Sci*. 2025;307:110883.

   doi: 10.1016/j.ijmecsci.2025.110883

5. Li T, Shen L, Xu H, Yu J. In-plane quasi-static compressive response and energy absorption mechanisms of vertex-based hierarchical re-entrant honeycombs. *Structures*. 2026;86:111430.

   doi: 10.1016/j.istruc.2026.111430

6. Lu J, Li Q, Qin R, *et al*. Enhanced energy absorption of assembled honeycomb system under in-plane compression. *Int J Mech Sci*. 2025;299:110404.

   doi: 10.1016/j.ijmecsci.2025.110404

7. Ma Y, Huang H, Deng X. Research on the in-plane energy absorption characteristics of the novel rotating self-similar star-shaped honeycomb structure. *Eng Fail Anal*. 2026;189:110696.

   doi: 10.1016/j.engfailanal.2026.110696

8. Wang X, Ma R, Cai J. Origami honeycomb material of designable deformation derived from Miura-ori patterns. *Smart Mater Struct*. 2026;35(3):035019.

   doi: 10.1088/1361-665X/ae4cdb

9. Xu S, Huang H, Fu Q, Guang X, Deng X. Octagonal hierarchical honeycomb with enhanced crashworthiness: Design, optimization, and performance under axial compression. *Structures*. 2026;86:111419.

   doi: 10.1016/j.istruc.2026.111419

10. Yu M, Wang Z, Song L, *et al*. Out-of-plane compression properties of a lightweight, high-strength and sustainable bamboo honeycomb sandwich structural material. *J Clean Prod*. 2025;498:145217.

    doi: 10.1016/j.jclepro.2025.145217

11. Zheng T, Wei Y, Song G, Tang C, Hao W. Compressive and Flexural Properties of a Novel Arc Honeycomb Structure. *Appl Compos Mater*. 2025;33(1):31.

    doi: 10.1007/s10443-025-10380-y

12. Zhou Q, Xu Z, Cui Y, Wang K, Wang B. Out-of-plane compression and energy absorption performance of twisted auxetic honeycomb tubes. *Int J Eng Sci*. 2026;220:104435.

    doi: 10.1016/j.ijengsci.2025.104435

13. Zhou Q, Xu Z, Cui Y, Wang K, Wang B, Wang B. Quasi-static lateral compression and energy absorption performance of dual-gradient auxetic honeycomb circular tube. *Thin-Walled Struct*. 2025;216:113683.

    doi: 10.1016/j.tws.2025.113683

14. Zhou Y, Li Z, Li X, Han S, Mo Z, Li J. Axial compression performance of honeycomb structure with diamond origami tube. *Constr Build Mater*. 2025;481:141602.

    doi: 10.1016/j.conbuildmat.2025.141602

15. Zhu C, Liu Y. Performance Design of Bio-Inspired Arc-Circular Honeycombs Under In-Plane Loading. *Biomimetics*. 2026;11(1):33.

    doi: 10.3390/biomimetics11010033

16. Du X, Qi L, Shi Y, *et al*. Dynamic Compressive Mechanical Behavior of a Novel Three-Dimensional Re-Entrant Honeycomb (3D-RH) Structure. *Materials*. 2025;18(22):5234.

doi: 10.3390/ma18225234

17. Liu G, Wang F, Tu Q, *et al*. An Euler Graph-Based Path Planning Method for Additive Manufacturing Thin-Walled Cellular Structures of Continuous Fiber-Reinforced Thermoplastic Composites. *Polymers*. 2025;17(23):3236.

    doi: 10.3390/polym17233236

18. Wang X, Li Z, Deng J, *et al*. Unprecedented Strength Enhancement Observed in Interpenetrating Phase Composites of Aperiodic Lattice Metamaterials. *Adv Funct Mater*. 2025;35(1):2406890.

    doi: 10.1002/adfm.202406890

19. Wang X, Li Z, Guo X, Li X, Wang Z. Superior damage tolerance observed in interpenetrating phase composites composed of aperiodic lattice structures. *Extreme Mech Lett*. 2024;72:102227.

    doi: 10.1016/j.eml.2024.102227

20. Hu Q, Zhang X, Zhang J, Lu G, Tse K. A review on energy absorption performance of auxetic composites with fillings. *Thin-Walled Struct*. 2024;205:112348.

    doi: 10.1016/j.tws.2024.112348

21. Quan C, Han B, Hou Z, Zhang Q, Tian X, Lu T. 3d printed continuous fiber reinforced composite auxetic honeycomb structures. *Compos Part B-Eng*. 2020;187:107858.

    doi: 10.1016/j.compositesb.2020.107858

22. Guo X, Xu Y, Wang X, *et al*. Design and fabrication of 3D isotropic chiral lattice metamaterials inspired by Kong-Ming locks. *Compos Struct*. 2026;120026.

    doi: 10.1016/j.compstruct.2025.120026

23. Wang Z, Chen X, Tian S, *et al*. An origami-inspired N-type core for all-composite sandwich construction: Enhanced mechanical performance and failure mechanisms. *Compos Struct*. 2025;377:119903.

    doi: 10.1016/j.compstruct.2025.119903

24. Cui X, Qiao Y, Hua L, Zhang H, Cui C. Out-of-plane compression performance of bionic gradient honeycomb structures. *Thin-Walled Struct*. 2026;227:115040.

    doi: 10.1016/j.tws.2026.115040

25. Ma J, Zhang H, Lee T, Lu H, Xie Y, San Ha N. Auxetic behavior and energy absorption characteristics of a lattice structure inspired by deep-sea sponge. *Compos Struct*. 2025;354:118835.

    doi: 10.1016/j.compstruct.2024.118835

26. Zhang C, Ba S, Zhao Z, Li L, Tang H, Wang X. Energy absorption characteristics of novel bio-inspired hierarchical anti-tetrachiral structures. *Compos Struct*. 2023;313:116860.

    doi: 10.1016/j.compstruct.2023.116860

27. Cui Z, Qi J, Tie Y, Zou T, Duan Y. Research on the energy absorption properties of origami-based honeycombs. *Thin-Walled Struct*. 2022;184:110520.

    doi: 10.1016/j.tws.2022.110520

28. Li Z, Yang Q, Fang R, Chen W, Hao H. Crushing performances of Kirigami modified honeycomb structure in three axial directions. *Thin-Walled Struct*. 2021;160:107365.

    doi: 10.1016/j.tws.2020.107365

29. Qi J, Li C, Tie Y, Zheng Y, Duan Y. Energy absorption characteristics of origami-inspired honeycomb sandwich structures under low-velocity impact loading. *Mater Des*. 2021;207:109837.

    doi: 10.1016/j.matdes.2021.109837

30. Yue Z, Han B, Wang Z, Yang M, Zhang Q, Lu T. Data-driven multi-objective optimization of ultralight hierarchical origami-corrugation meta-sandwich structures. *Compos Struct*. 2022;303:116334.

    doi: 10.1016/j.compstruct.2022.116334

31. Jin J, Wu S, Yang L, *et al*. Ni–Ti multicell interlacing Gyroid lattice structures with ultra-high hyperelastic response fabricated by laser powder bed fusion. *Int J Mach Tool Manu*. 2024;195:104099.

    doi: 10.1016/j.ijmachtools.2023.104099

32. Benedetti M, Du Plessis A, Ritchie RO., Dallago M, Razavi N, Berto F. Architected cellular materials: A review on their mechanical properties towards fatigue-tolerant design and fabrication. *Mat Sci Eng R*. 2021;144:100606.

    doi: 10.1016/j.mser.2021.100606

33. Wang P, Yang F, Zheng B, *et al*. Breaking the Tradeoffs between Different Mechanical Properties in Bioinspired Hierarchical Lattice Metamaterials. *Adv Funct Mater*. 2023;33(45):2305978.

    doi: 10.1002/adfm.202305978

34. Wang X, Li X, Li Z, Wang Z, Zhai W. A ribbed strategy disrupts conventional metamaterial deformation mechanisms for superior energy absorption. *Virtual Phys Prototyp*. 2024;19(1):e2337310.

    doi: 10.1080/17452759.2024.2337310

35. Yao S, Zhou H, Gao T, Chen F, Wang Z, Liu K. Origami-inspired highly impact-resistant metamaterial with loading-associated mechanism and localization mitigation. *Int J Mech Sci*. 2025;290:110114.

    doi: 10.1016/j.ijmecsci.2025.110114

36. Lei Z, Liu J, Guo Z, *et al*. UHPC-honeycomb-lattice composite structure for vessel collision fendering: Impact characterization and design framework. *Eng Struct*. 2026;347:121697.

    doi: 10.1016/j.engstruct.2025.121697

37. Lei Z, Liu J, Guo Z, *et al*. Metal honeycomb skeleton

reinforced foam concrete: Mechanical properties, reinforcement mechanism and optimal design. *Eng Struct*. 2025;341:120827.

doi: 10.1016/j.engstruct.2025.120827

38. Lei Z, Gao F, Di H, Liu J, Wang Z. Enhancing resistance of honeycomb sandwich panel under local impact through face sheet-core matching relationship. *J Cent South Univ*. 2025;32(8):3136-3149.

doi: 10.1007/s11771-025-6028-x

39. Niu H, Lu J, Qin R, *et al*. A self-locked chiral honeycomb: In-plane compression behavior and energy absorption. *Eur J Mech A-Solid*. 2025;111:105580.

doi: 10.1016/j.euromechsol.2025.105580

40. Zhang Q, Jia J, Dong L, Zhi G. In-plane bidirectional quasi-static compression behavior of a novel multi-step star-isosceles triangular honeycomb. *Mater Des*. 2025;259:114836.

doi: 10.1016/j.matdes.2025.114836

41. Cui C, Chen T, Qiao Y, *et al*. Deformation response and enhanced energy absorption capacity of a novel re-entrant honeycomb with hybrid structures and bi-material under in-plane compression. *Compos Struct*. 2025;367:119268.

doi: 10.1016/j.compstruct.2025.119268

42. Liu B, Zou J, Yin H, Gu X, Yang Y, Chen X. Compression performance evaluation of a novel origami-lattice metamaterial. *Int J Mech Sci*. 2024;273:109220.

doi: 10.1016/j.ijmecsci.2024.109220

43. Peng X, Zhou K, Han Y, Jia W, Li J, Jiang S. Compression performance analysis of hexagonal and re-entrant hybrid honeycomb structures. *Polym Test* 2025;145:108745.

doi: 10.1016/j.polymertesting.2025.108745

44. Yuan S, Wei Y, Gong J, Tang C, Hao W. Compressive behavior of improved star-shaped honeycomb multi-cell structures: Experiments and simulations. *Mech Adv Mater Struct*. 2025;33(1):2457126.

doi: 10.1080/15376494.2025.2457126

45. Yang H, Li Z, Liu Y, *et al*. Comprehensive experimental study on the corrugated honeycombs with multidirectional load-bearing and energy absorption performance under various loading conditions. *Thin-Walled Struct*. 2025;216:113765.

doi: 10.1016/j.tws.2025.113765

46. Huang W, Zhang Y, Xu Y, Xu X, Wang J. Out-of-plane mechanical design of bi-directional hierarchical honeycombs. *Compos Part B-Eng*. 2021;221:109012.

doi: 10.1016/j.compositesb.2021.109012

47. Zhang Z, Chen Z, Hu X, Cai W. Out-of-Plane compressive performance of a novel bio-inspired honeycomb with sinusoidal rib: integrated theoretical and numerical analysis. *Results Eng*. 2025;28:107314.

doi: 10.1016/j.rineng.2025.107314

48. Lin K, Gu D, Hu K, *et al*. Laser powder bed fusion of bio-inspired honeycomb structures: Effect of twist angle on compressive behaviors. *Thin-Walled Struct*. 2020;159:107252.

doi: 10.1016/j.tws.2020.107252

49. Chen L, Cui C, Cui X, Lu J. Cuttlebone-inspired honeycomb structure realizing good out-of-plane compressive performances validated by DLP additive manufacturing. *Thin-Walled Struct*. 2024;198:111768.

doi: 10.1016/j.tws.2024.111768

50. Cui C, Chen T, Chen L, Cui X, Wang X, Yan H. Double-layer helix honeycomb structure with optimal torsion angle achieving excellent compressive performances. *Mater Today Commun*. 2024;40:109562.

doi: 10.1016/j.mtcomm.2024.109562

51. Guo C, Cheng X, Lu L, Pan L. Multi-combination structural optimization design of polymer honeycombs under quasi-static compression. *Int J Solids Struct*. 2025;321:113586.

doi: 10.1016/j.ijsolstr.2025.113586

52. Guo C, Cheng X, Lu L, Pan L, Wang J. Energy absorption of central self-similar honeycombs under quasi-static axial load. *Int J. Mech Sci*. 2024;274:109264.

doi: 10.1016/j.ijmecsci.2024.109264

53. Wang S, Pei W, Jin S, Yu H. Numerical and theoretical analysis of the out-of-plane crushing behavior of a sinusoidal-shaped honeycomb structure with tunable mechanical properties. *Structures*. 2024;61:106147.

doi: 10.1016/j.istruc.2024.106147